IEEE Access
Multidisciplinary | Rapid Review | Open Access Journal

Received June 24, 2019, accepted July 19, 2019, date of publication July 24, 2019, date of current version August 6, 2019.

Digital Object Identifier 10.1109/ACCESS.2019.2930873

Implementation of Human-Like Driver Model Based on Recurrent Neural Networks

AOXUE LI, HAOBIN JIANG, JIE ZHOU, AND XINCHEN ZHOU
School of Automotive and Traffic Engineering, Jiangsu University, Zhenjiang 212013, China

Corresponding author: Aoxue Li (ujsliaoxue748@163.com)

This work was supported in part by the National Natural Science Foundation of China under Grant 51675235 and Grant 51605199, and in part by the Postgraduate Research and Practice Innovation Program of Jiangsu Province under Grant KYCX17_1812.

ABSTRACT Driver model is the most basic and important model for moving direction control of autonomous vehicles and it has been extensively studied from the perspective of precision and robustness of control, driving safety, and riding comfort. However, human-like driver model is a rarely mentioned research issue. In this paper, we first establish three preview-based driver models in PreScan+Simulink and collect human drivers' steering data on four two-way and two-lane free curved roads with 20 experienced drivers and one experimental vehicle under four specified speeds. Then, the similarities between steering wheel angles of preview-based models and those of human drivers are compared through dynamic time warping (DTW). From the calculation results of DTW and analysis of human drivers' gaze positions, it shows that the preview-based models are hard to reflect the characteristics of human drivers' maneuver. To this end, we propose a human-like driver model based on the continuity of human drivers' steering wheel angles. The experienced drivers' steering wheel angels are modeled with three different kinds of multivariate multi-step recurrent neural networks (RNNs) and the inputs of models are historical speeds, historical road curvatures, future road curvatures, and historical steering wheel angles, as well as the outputs are future steering wheel angles. By comparing the three RNN-based driver models with different configuration structures and historical steps, it is found that the long short-term memory (LSTM) model has the best prediction performance in validation and testing period. In this way, a data-driven human-like driver model is developed to generate human-like steering wheel angles on curved roads.

INDEX TERMS Human-like driver model, curved roads, RNN, LSTM, experienced drivers.

I. INTRODUCTION

In recent years, the development of autonomous vehicles (AVs) have attracted the world's attention. The deployment of AVs will also have important impacts on the future transportation system [1], the way people travel [2], and the future development trend of automobile industry. It is believed that AVs are more likely to be accepted if they drive safely, comfortably, and behave like human drivers [3], [4]. Driving safety and ride comfort are two common considerations in AV technologies, but human-like driving is rarely studied. The importance of human-like driving is that in the initial stage of the popularity of AVs, AVs and human-driven vehicles need to share the roads. The rationale is not that human-like driving would somehow be superior, but rather that humans will find it easier to interact and feel at ease with AVs in such case [5].

Driver model is the most basic and important model for driving direction control (or lateral control) of AVs. The main three groups of methodology used to develop driver models are classical control theory, modern control theory, and intelligent control theory [6]. In classical control theory, the system is represented using transfer functions, and preview control driver model is the typical and most widely used driver model. As early as 1980, MacAdam [7] developed an optimal preview control algorithm and successfully applied this algorithm to lane tracking and lane changing tasks. And since that time, various kinds of preview-based driver models have been developed based on different assumptions about the drivers' preview positions. Preview-based driver models represented the driver as an optimal preview controller, constructing a path error functional by previewing the road over a known preview distance, and minimizing the

The associate editor coordinating the review of this manuscript and approving it for publication was Malik Jahan Khan.

differences between the previewed path points and the corresponding estimated lateral positions of the vehicle over the preview distance [8]. Model predictive control (MPC) is another well-known method to model lateral control system of AVs, and it uses modern control theory to represent the human-vehicle-road closed-loop system in state space [9]. One thing in common with the aforementioned methods is that they are all based on tracking control theory, so a tracking trajectory (or desired trajectory) needs to be set in advance. And lane centerlines are often used directly as the desired trajectories. Of course, many studies adjusted the parameters in the driver models by least squares parameter identification to make the trajectories of AVs close to that of human drivers' [10]. The parameters of these models are difficult to modify in order to characterize different driving behaviors; instead, the model must be retrained using new data to capture new roads, new driving conditions, and new driver types. In practical applications, generalization performance is the biggest drawback of these two kinds of driver models. When developing driver models with intelligent control theories, neural network [11], fuzzy logic [12], and hidden Markov model (HMM) [13] are commonly used. Neural network and fuzzy logic have very good non-linear approximation function. When embedded in preview-based driver model, they can flexibly adjust model parameters. However, they still need to work with other mathematical models like vehicle dynamics model, preview model, and feedback model. The driving pattern primitives consisting of states of the environment, vehicle, and driver are symbolized by HMMs, which can be used for both recognition and generation of the driving behaviors. Since the driver behavior is proposed of stochastic model, the prediction steps of HMM are relatively short. This means that as the forecast steps increase, the predicted performances of the HMM driver model will gradually decrease.

In this paper, we firstly establish three preview-based driver models in PreScan [14] and Simulink. To compare the differences between preview-based driver models and experienced drivers, the steering wheel angles, trajectories, speeds, and other driving data of experienced drivers are collect from a field test on four free curved roads. Twenty participants and one experimental vehicle are included in the experiments. By placing virtual landmarks on the experimental roads, the driving data of experienced drivers are transformed into sequential data with a uniform format. DTW [15] is used to compare the similarities between preview-based driver models and human drivers, and the calculation results show that the differences between the steering wheel angles of experienced drivers and those of preview-based models are big. Finally, the inherent disadvantages of the preview-based driver models and the needs of human-like driving for AVs that motivate us to build a human-like driver model. The human-like driver model is based on three different multivariate multi-step recurrent neural networks, and the inputs of model are historical speeds, historical road curvatures, future road curvatures, and historical steering wheel angles, as well as the outputs are future steering wheel angles. The proposed human-like driver model in this paper learns from experienced drivers directly which aiming at realizing AVs' human-like driving on curved roads. The contributions of this paper include the following:

1) Three preview-based driver models are built in PreScan+Simulink and DTW is introduced to calculate the similarities between the steering wheel angles of simulation results and those of experienced drivers.
2) A comprehensive field test with twenty experienced drivers is conduct on four curved roads with different curvatures under four specified speeds and the driving data are able to reflect the characterization of human driving on curved roads.
3) Based on recurrent neural networks, we propose a human-like driver model on curved roads. The model can generate human-like steering wheel angles and its performance is evaluated with different hidden layers and historical steps.

The remainder of the paper is organized as follows. Section II outlines related studies. Three most classical preview-based driver models are presented in Section III and the simulation setup of the preview-based driver models in PreScan+Simulink are illustrated in Section IV. The experiment setup and details for human drivers' driving data collection are introduced in Section V. Section VI presents data processing and comparisons between preview-based driver models and human drivers. In section VII, a human-like driver is developed with three different kinds of recurrent neural networks. In Section VIII, we present all the hyperparameter settings of the human-like driver and validate as well as test its effectiveness. Finally, conclusions are made in Section IX.

II. RELATED WORK

For driver steering behavior, studies have been conducted in regard to modeling physical human characteristics, sensory information, and perception and behavioral aspects. Preview-based models [16] are the most typical driver models, and they use compensatory transfer functions based on heading errors at a preview distance. These preview-based driver models provide many of the features expected in a model of the human driver, namely preview of the future road path, feedback of vehicle states, control based on knowledge of the vehicle dynamics, and parameters to specify the control priorities of the driver. When using single-point preview models, the first concern in choosing parameter values is to set a preview distance (or preview time) which is reasonable [17]. Since if the preview point is a long distance in front of the vehicle, it will be inappropriate to act on the preview information at the time of its acquisition and the information has gone by the time it is useful. On the other hand, if the preview point is very close to the vehicle, control will necessarily be very poor. Aware of the problems existing in the single-point preview driver model, many scholars have proposed the two-point preview driver model. Salvucci and Gray [18] proposed a two-level model of steering control

that used the perceived visual direction of two salient visual points, a ''near point'' in the near region and a ''far point'' in the far region of the roadway. Based on field test data, You *et al.* [6] presented that two-point visual driver model captures realistic driving behavior with time-varying parameters. However, Sharp et al. [19] believed drivers not only acquire path preview information by looking ahead of the vehicle, but also have state error information from the relation between the present position and that desired. By weighting and summing all the estimated errors, they proposed a multi-point preview driver model. In addition to the parameters of the control system, drivers' reaction time t_d and neuromuscular delay time t_h are often considered to be human properties. Auto-regression moving average with exogenous inputs (ARMAX) [20], Fourier coefficient method (FCM) [21], and least square method [22], [23] are always used for identifying driver's steer characteristics. However, to the best as we know, no research has proved that the identified parameters are the real physiological reaction time of human drivers.

To further improve the performance of the preview-based driver models, fuzzy logic and artificial neural network (ANN) are often embedded in the models. A fuzzy rule-based neural network model was proposed in [24] to simulate driver behavior in terms of longitudinal and lateral actions. In [25], the collision avoidance maneuver is performed using fuzzy controllers for AVs to mimic human behavior and reactions. Lin *et al.* [26] proposed a ANN-based driver handling behaviour model with the position, velocity and acceleration of the vehicle used as the input and the front wheel steer angle considered as the desired output of the trained network. Caoet *et al.* [27] developed a new vehicle path-following strategy based on the preview optimal simple artificial neural network (POSANN). Model predictive control (MPC) is an efficient trajectory tracking control algorithm and is often used to build driver model [28]. Based on a linear optimal path tracking controller, Ungoren and Peng [29] proposed an adaptive lateral driver model using MPC. Cole *et al.* [9] compared the method of MPC with receding horizon linear quadratic (LQ) and infinite horizon LQ. The time-variant predictive control method was applied in [30] to model the driver steering skill. Most of the aforementioned models were designed to control steering wheel for specific applications. However, none of these studies took into account each driver's desired trajectory as part of their driver models. Their mathematical formulations were used for precise control so the physical characteristics of human drivers were ignored.

With the study and development of machine learning, especially deep learning, data-driven modeling methods are becoming more and more widely used. Bojarski *et al.* [31] trained a convolutional neural network (CNN) to map raw pixels from a single front-facing camera directly to steering commands of AVs and this end-to-end approach proved surprisingly powerful. Similarly, Chi and Mu [32] designed a convolutional long short term memory (Conv-LSTM) neural network to predict the due wheel angle for a AV. Imitation learning was applied in [33] to learn car racing behaviors from the data of human drivers. NN-based model has accurate prediction performance and convenient model structure, and the generalization ability of NN-based model is very good [34]. What's more, due to the direct use of drivers' maneuver data to build the driver model, the obtained driver model has a high similarity with human drivers. We believe that the driving behavior of human drivers under normal conditions mainly depends on their driving experience and driving habits. This paper proposes a human-like driver model based on three different kinds of recurrent neural networks: standard recurrent neural network (RNN) [35], long short-term memory (LSTM) [36], and gated recurrent unit (GRU) [37]. The driver model can generate human-like steering wheel angles on free curved roads. The modeling work in the paper is based on normal driver conditions. Abnormal driver condition variations caused by factors such as physiological conditions, stress, and distractions are not considered.

III. PREVIEW-BASED DRIVER MODEL

One may consider ''driving an AV'' intuitively as a control task and this may be a reason why control theory based driver models have been successful. From a control theory point of view, the crucial ability of the driver model is to follow a specified course given by a desired trajectory. In order to study and simulate the characteristics of driving behaviors in different traffic conditions, many types of driver models are built. The three most classical driver models are single-point preview driver model, two-point preview driver model, and multi-point preview driver model. However, these models cannot really reflect the characteristics of human drivers' maneuver when controlling the steering wheel angles. To this end, we propose a human-like driver model based on recurrent neural networks.

A. SINGLE-POINT PREVIEW DRIVER MODEL

Taking into account the perception and delay behavior of humans during the steering process, single-point preview driver model is proposed. The steering strategy can be understood as the driver always attempts to minimize the error Δy_p between the vehicle's actual trajectory and desired trajectory, as shown in Figure 1(a). The distance L ahead the vehicle is called ''preview distance''. Most of the time, we use ''preview time'' t_p ($t_p = L/v$) to indicate driver's preview behavior.

In terms of transfer functions, single-point preview driver model can be illustrated in a more general form by the control loop of Figure 2. In the preview segment $P(s)$, the driver previews a distance ahead the desired trajectory $f(t)$ with the output f_e. $H(s)$ donates the control characteristics of the driver, $G(s)$ the transfer function of the vehicle model, and $B(s)$ the feedback function.

$e^{t_p s}$ donates driver preview transfer function, $e^{-t_d s}$ the natural reaction delay transfer function, and $\frac{1}{1+t_h s}$ the inertial delay of driver hand and vehicle steering system.

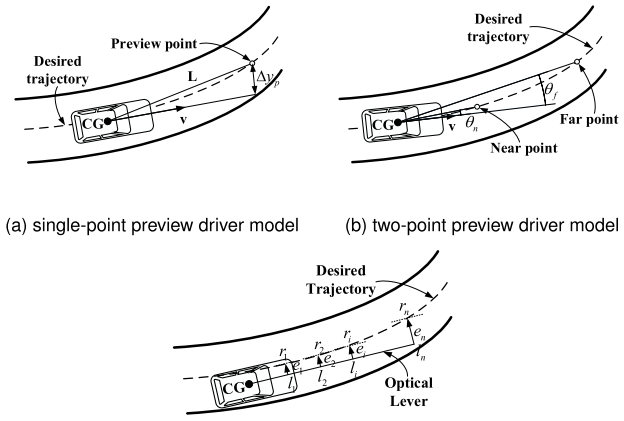

(a) single-point preview driver model (b) two-point preview driver model

(c) multi-point preview driver model

FIGURE 1. Three different preview-based driver models.

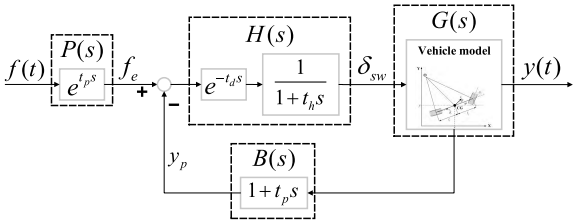

FIGURE 2. Basic control loop of preview tracking models.

What's more, t_d is the reaction time of the driver, t_h the neuromuscular delay time, δ_{sw} the steering angle of the vehicle, $y(t)$ the output of the vehicle, and y_p the driver's predicted lateral trace. In general, the control structure of a driver model coupled with a vehicle coincides with the preview-follower theory.

B. TWO-POINT PREVIEW DRIVER MODEL

A steering control model that uses the perceived visual direction of two salient visual points, a "near point" in the near region and a "far point" in the far region of the roadway, is propose as the two-point preview driver model. As shown in Figure 1(b), θ_f donates the angle between the driver's sight direction on the far point and vehicle' heading direction, and θ_n the angle between the driver's sight direction on the near point and vehicle's head direction. The control law of steering angle is:

$$\dot{\delta} = k_f\dot{\theta}_f + k_n\dot{\theta}_n + k_I\theta_n. \tag{1}$$

When modeling two-point driver model, we always use the discrete formulation:

$$\Delta\delta = k_f\Delta\theta_f + k_n\Delta\theta_n + k_I\theta_n\Delta t, \tag{2}$$

where k_f, k_n, and k_I are gain parameters, and δ is the ideal steering angle. The distance from the center of gravity (CG) to the near point is donated as L_n, and the distance from CG to the far point is L_f. The reaction time and neuromuscular delay time are also included in Simulink model. Two-point preview driver model assumes that the driver aims to keep the sight angles θ_n and θ_f to these points stationary, and at the same time attempting to reduce the near point angle to zero.

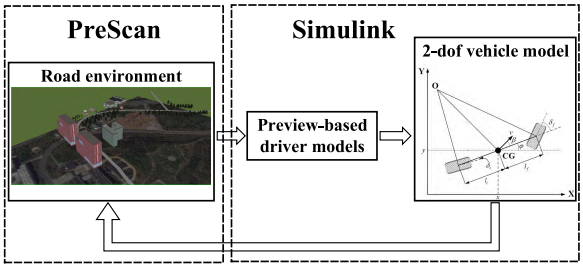

FIGURE 3. Construction of simulation in PreScan and Simulink.

C. MULTI-POINT PREVIEW DRIVER MODEL

The multi-point preview driver model also makes use of the preview-follower theory. However, instead of calculating its steering wheel angle as a weighted sum of current and previewed trajectory deviations e_i along a forward optical lever, multi-point preview driver model extends a preview time t_p ahead (as illustrated in Figure 1(c)), and calculates the current deviation e_ψ between vehicle and trajectory heading:

$$\delta = k_\psi e_\psi + k_1 e_1 + k_p\Sigma_{i=2}^{n} k_i e_i, \tag{3}$$

where k_ψ, k_1, and k_p are gain parameters, δ the ideal steering angle, and n the number of preview points. Additionally, to allow for a fair comparison with the other models, reaction time t_d and neuromuscular delay time t_h are added to Equation 3.

IV. SIMULATION

In order to compare the differences between the traditional preview-based driver models and human drivers on the same road, three preview-based driver models (single-point preview, two-point preview, and multi-point preview driver models) are simulated in PreScan+Simulink, respectively. PreScan is an active experimental platform [38], and it is able to build scenes based on the actual road environment and sensor model.

A. CONSTRUCTION OF SIMULATION

PreScan and Simulink are used to build the simulation environment. Each simulation model consists of three parts: vehicle model, road environment, and driver model. The main function of PreScan is to build the road environment, while the vehicle model and driver model are connected to PreScan via Simulink.

A total of four roads are built in PreScan, each of which is the same as the experimental road in field test. For the vehicle dynamics model, we use a 2-degree-of-freedom (dof) bicycle model [39]:

$$m\dot{v} + (\frac{2C_f + 2C_r}{u})v + (mu + \frac{2l_fC_f - 2l_rC_r}{u})r = \frac{2C_f\delta_{sw}}{n_{sw}}, \tag{4}$$

TABLE 1. Parameters of the vehicle model.

l_f	distance from CG to front axle	1.110 m
l_r	distance from CG to rear axle	1.478 m
m	total mass	1420 Kg
I_z	yaw moment of inertia	1810 Kg·m^2
C_f	front cornering stiffness	153000 N/rad
C_r	rear cornering stiffness	82000 N/rad
n_{sw}	steering gear ratio	17

TABLE 2. Parameters of three preview-based models.

Parameters	Allowed range	Used by models
t_p	[1, 4.5] s	Single-point & Two-point preview
t_d	[0, 1] s	All
t_h	0.2 s	All
L_f	[10, 30] m	Two-point preview
L_n	[30, 70] m	Two-point preview
k_f	[5, 30]	Two-point preview
k_n	[5, 30]	Two-point preview
k_I	[1, 10]	Two-point preview
k_ψ	[5, 30]	Multi-point preview
k_1	[5, 30]	Multi-point preview
k_p	[1, 10]	Multi-point preview

$$I_z\dot{r} + (\frac{2l_fC_f - 2l_rC_r}{u})v + (\frac{2l_f^2C_f + 2l_r^2C_r}{u})r = \frac{2l_fC_f\delta_{sw}}{n_{sw}}, \tag{5}$$

where u donates the longitudinal vehicle velocity, v the lateral vehicle velocity, r the yaw rate, and δ_{sw} the steering wheel angle. The parameters of the vehicle model are shown in Table 1.

In order to match the speed requirement in the field test, a proportional–integral–derivative controller (PID controller) is used to control the vehicle speed during simulation so that it maintains a constant value throughout the curves. The proportional gain K_p is 20, integral gain K_i is 0.3, and derivative gain K_d is 3.065.

B. PARAMETERS OF THE THREE PREVIEW-BASED DRIVER MODELS

As illustrated in Section III-A, B, and C, each preview-based model has its own parameters, which directly affect the performance of the driver models [40]. For each parameter, the allowed range is presented in Table 2, together with information on which models made use of the parameters. Additionally, the lane centerline of each road is set as the desired trajectory for three preview-based driver models.

It should be noted that in the simulation, the interval of t_p and t_d are 0.1 s, the interval of L_f and L_n are 10 m, the interval of k_f, k_n, k_ψ, and k_1 is 5, and the interval of k_I and k_p is 1. We want to compare the steering wheel angles obtained by preview-based models with those of human drivers by traversing all parameters.

C. DYNAMIC TIME WARPING

After the simulation is completed, we use dynamic time warping (DTW) [41] to calculate the similarities between the steering wheel angles of simulation results and those of experienced drivers. Before comparing, the original sequential data should be normalized. For $F = \{f_1, f_2, \cdots, f_i, \cdots, f_m\}$, the z-normalization algorithm:

$$\hat{f}_i = \frac{f_i - \mu}{\sigma}, \tag{6}$$

where μ and σ donate mean and standard deviation of F. The normalization result of F is $\hat{F} = \{\hat{f}_1, \hat{f}_2, \cdots, \hat{f}_i, \cdots, \hat{f}_m\}$.

For two sequential data of steering wheel angles $F = \{f_1, f_2, \cdots, f_i, \cdots, f_m\}$ and $G = \{g_1, g_2, \cdots, g_j, \cdots, g_n\}$, the DTW distance between them is denoted by $DTW(F, G)$:

$$DTW(F, G) = \sqrt{D(F, G)}, \tag{7}$$

$$D(F, G) = dist(f_i, g_j) + min \begin{cases} D(f_{i-1}, g_j) \\ D(f_i, g_{j-1}) \\ D(f_{i-1}, g_{j-1}), \end{cases} \tag{8}$$

where $D(f_0, g_0) = 0$, $D(f_i, g_0) = D(f_0, g_j) = \infty$, $i = 1, 2, \cdots, m$, and $j = 1, 2, \cdots, n$. Typically the Euclidean distance is used, so $dist(f_i, g_j) = (f_i - g_j)^2$. In this paper, on the same road, the lengths of F and G are the same (i.e. $m = n$).

V. FIELD TEST

To collect the steering wheel angles of experienced drivers on curved roads and further make comparisons with preview-based driver models, we conduct a field test on four curves with different curvatures. The participants, experimental equipments, experimental roads, and procedures are detailed in the following subsections.

A. PARTICIPANTS

We recruited 5 driving instructors, 5 bus drivers, and 10 taxi drivers as the representatives of experienced drivers. Experienced drivers have excellent driving ability and relatively stable driving style. The age, gender, driving experience, and annual vehicle kilometers traveled (AVKT) are presented in Table 3.

TABLE 3. Details of all participants.

Number	Average age (years)	Gender (Femal/Male)	Driving experience (years)	AVKT (kilometers)
J1-J5	48.5	1/4	23.4	4.6×10^4
J6-J10	38.5	0/5	13.6	7.6×10^4
J11-J20	39.9	3/7	15.2	4.9×10^4

Four of the experienced drivers are female and the average age all participants is about 41.7. The average AVKT of all the participants is 4.5×10^4 km/year and the average driving experience is about 16.8 years.

B. EXPERIMENTAL VEHICLE AND EXPERIMENTAL EQUIPMENTS

In this study, one SKODA Octavia is used as the experimental vehicle (as shown in Figure 4). To record vehicle positions, a differential GPS system and a integrated positioning

FIGURE 4. Experimental vehicle and experimental equipments.

FIGURE 5. Test fields with four curved roads.

TABLE 4. Details of the four experimental roads.

Number	Radius of curvature (m)	Deflection angle (°)
R1	252	94.2
R2	100	85.2
R3	136	27.4
R4	226	99.8

system (INS) are installed on the top of the experimental vehicle. What's more, a measurement steering wheel (MSW) is mounted on the steering wheel of the original vehicle to measure the steering wheel angles.

The acquisition accuracy of the GPS/INS is ± 0.01 m and the sampling frequency is 20 Hz. The speed, longitude, latitude, time, row, pitch as well as other data could be collected through the NovAtelConnect_1.4.0 software. The type of MSW is Kistler CMSWB, the measurement range of steering angle is ± 1250 ∘, and the accuracy of MSW is ± 0.1 ∘.

C. TEST FIELDS

The experiments are conducted on four two-lane roadways, with one lane in each direction (as shown in Figure 5).

Each curve consists of two straight line segments, two transition curve segments, and one circular curve segment. The radius of curvature r and deflection angle α of each experimental road's circular curve segment are illustrated in Table 4.

D. PROCEDURE

Each experimental road has two moving directions, experienced drivers drive on each moving direction five times with four specified vehicle speeds, 20 km/h, 30 km/h, 40 km/h, and 50 km/h, respectively. Before each test, the experienced drivers are informed about the required vehicle speed for the current test and asked to keep this speed as much as possible during their driving. All participants are explicitly informed about the contents of the experiment. Since there is only one experimental vehicle and the experimental roads are separated, the participants take turns to carry out their tests and each participant's test time is about 2 hours.

VI. DATA PROCESSING AND COMPARISON RESULTS

The field test collects a total of 3200 pieces of data, among which the valid data are 2976 pieces. In the course of the field test, experienced drivers control the vehicle speed very well, but the speed is not a fixed value on the whole curve. We want to project the steering wheel angle to the position of the road, that is, to plot the figure of steering wheel angle changing with the length of the curve (as shown in the top of Figure 6). In order to achieve the above purpose, we process the collected data in two steps: First, determine the position of the vehicle on each virtual landmark; Then, find the corresponding steering wheel angle and vehicle speed. The calculation process of vehicle speeds, vehicle position, road curvature, and steering wheel angles are depicted in the following subsections.

A. CALCULATE VEHICLE POSITION

Due to the differences of vehicle speeds, there is a certain degree of inconsistency between each original trajectory (e.g. two trajectories in Figure 6). So a lot of virtual landmarks are placed along the separation line of each experimental road. The virtual landmarks are only used for calculating the vehicle position. The distance between two neighboring virtual landmarks of each experimental road is 1 m.

The GPS sampling point closest to the virtual landmark is selected as the feature point. As an example, see Figure 6 for two sample trajectories, $\{\cdots, P_{i-1}, P_i, P_{i+1}, \cdots\}$, and $\{\cdots, Q_{j-2}, Q_{j-1}, Q_j, Q_{j+1}, Q_{j+2}, \cdots\}$.

For each virtual landmark $VL_k, k = 1, 2, \cdots, N$, we define the following neighborhood:

$$D_k := \{s | ||VL_k - s|| \leq R\}, \tag{9}$$

where R is the radius and we choose R =5 m in this study. Then we searched for all GPS sampling points in the calculation domain.

For trajectory $\{\cdots, P_{i-1}, P_i, P_{i+1}, \cdots\}$, it has only one GPS sampling point in the computation domain and P_i is the feature point. However, trajectory $\{\cdots, Q_{j-2}, Q_{j-1}, Q_j, Q_{j+1}, Q_{j+2}, \cdots\}$ has two sampling points in the calculation domain. Multiple sampling points may also occur during the actual calculation. When two or more sampling points appear, the linear distance between each sampling point and virtual landmark VL_k is calculated first. And it is found that:

$$\overline{Q_{j+1}VL_k} < \overline{Q_jVL_k}. \tag{10}$$

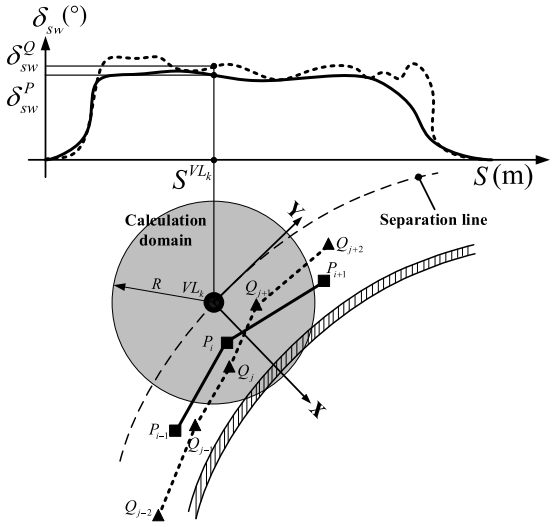

FIGURE 6. Calculations of vehicle positions.

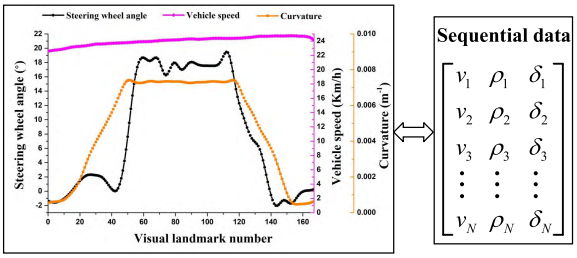

FIGURE 7. Sequential data of one test on experimental road R3.

So Q_{j+1} is selected as the feature sampling point. Through the above calculation, each trajectory has one unique feature point at each virtual landmark.

B. CALCULATE STEERING WHEEL ANGLE

Based on the feature point at each virtual landmark, we can find the vehicle speed and steering wheel angle corresponding to the feature point. All the data we collected can be transformed into sequential data with a uniform format.

Figure 7 illustrates the data processing of one test on the inside lane of experimental road R3. The length of experimental road R3 is 167 m, so N (N donates the maximum number of visual landmark) is 168. It should be noted that when the steering wheel rotates clockwise, the steering wheel angles are defined as positive, and when the steering wheel rotates counter-clockwise, the steering wheel angles are negative.

C. PREVIEW MODELS VERSUS EXPERIENCED DRIVERS

We get a total of N steering wheel angle data for human drivers in one specified speed. We will use the single-point preview model as an example to introduce the specific process of calculating similarity using DTW. For example, signal-point preview driver model totally has M sets of parameters. Through simulation, we can get M pieces of steering wheel angle sequence data. For one piece steering wheel angle data i, its similarity to the steering wheel angles of all experienced drivers is defined as:

$$DTW_i = \frac{1}{N}\sum_{j=1}^{N} DTW(i,j), \quad j = 1, 2\cdots, N, \qquad (11)$$

where DTW_i donates the similarity of steering wheel angles between i-th signal-point preview driver model and experienced drivers. We also use DTW_{max}, DTW_{min}, and DTW_{ave} to present the maximum, minimum and average values of DTW_i:

$$\begin{cases} DTW_{max} = maxDTW_i \\ DTW_{min} = minDTW_i \\ DTW_{ave} = \dfrac{1}{M}\sum_{i=1}^{M} DTW_i, \end{cases} \quad i = 1, 2\cdots, M. \qquad (12)$$

Table 5 illustrates the calculation results of similarities between the steering wheel angles of three preview-based models and those of experienced drivers on experimental road R2 when the specified speed is 40 km/h.

It can be seen that two-point and multi-point preview driver models are more similar to human drivers in general. In order to show the similarities more intuitively, we find the most similar pair ($DTW* = min_{i=1}^{M} min_{j=1}^{N} DTW(i,j)$) of steering wheel angles and show them in Figure 8.

It should be noted that the steering wheel angles of experienced drivers in the three sub-figures of Figure 8 do not belong to the same driver. Obviously, the differences between the steering wheel angles of experienced drivers and those of three preview-based models are very big. It is difficult to show different driving habits and driving characteristics of different drivers with only one preview-based driver model.

TABLE 5. Similarities between preview-based driver models and experienced drivers (specified speed: 40 km/h).

		Signal-point	Two-point	Multi-point
Experienced drivers	DTW_{ave}	4.3423	3.5602	2.9397
	DTW_{max}	6.1780	6.4784	4.8861
	DTW_{min}	2.9858	2.3172	2.3639

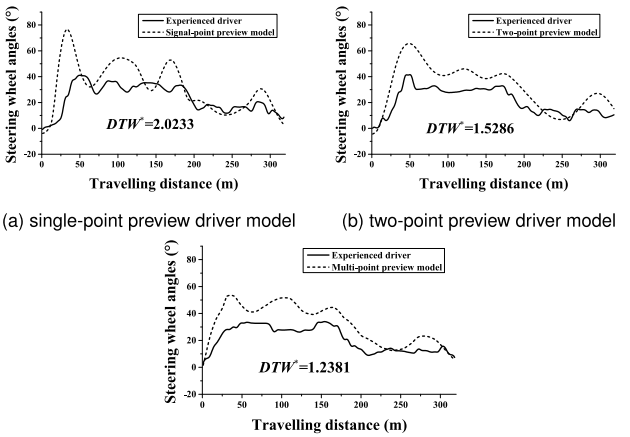

(a) single-point preview driver model (b) two-point preview driver model

(c) multi-point preview driver model

FIGURE 8. The most similar pair of steering wheel angles between preview-based models and experienced drivers.

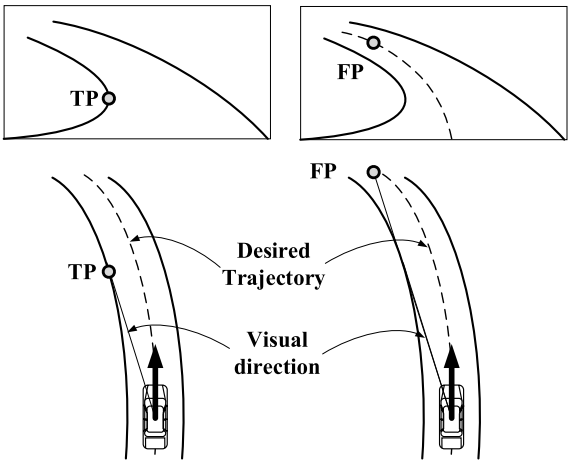

FIGURE 9. TP and FP reference points in the visual field.

VII. HUMAN-LIKE DRIVER MODEL

A. GAZE POSITIONS OF HUMAN DRIVERS

The preview-based driver models imitate the forward-looking characteristics of human drivers when driving. The selection of preview points has a great influence on the performance of the model. Common sense suggests that drivers should ''keep their eyes on the road'' and ''look where they are going''. Indeed, measurement of drivers' eye movements has shown that during curve negotiation gaze is focused in a remarkably small region in the visual field. One mainstream model is ''tangent point model'' [42], which posits that drivers' gaze position is the tangent point (TP). TP model quickly became the default account of how vision is used during curve negotiation. More recent studies, however, believe drivers seek out target points on the road surface that they desire their locomotor trajectory to fall on—their future path (FP) [43].

Single-point preview, two-point preview and multi-point preview driver models are based on preview-follow theory. However, there is no evidence to determine whether the TP or the FP is the ''real'' target that drivers always look at. TP and FP are often only of reference value for preview-based driver models. This leads to a very serious drawback of the above three driver models: It is difficult to determine the preview distance, or it is difficult to select a suitable preview distance in different scenarios. What's more, the preview-based driver models rely heavily on the pre-set desired trajectory, which is generally considered as the centerline of the lane. However, there is no evidence that human drivers have a clear desired trajectory in their mind when driving. To summarize, limited by the preview-follow theory, the preview models are difficult to reflect the actual personality characteristics of different human drivers.

B. MODEL ESTABLISHMENT

Since preview-based driver models are difficult to make AVs behave like human drivers, we propose a human-like driver model on curved roads. The driver model considered in this paper is on free-roads. We believe that when driving

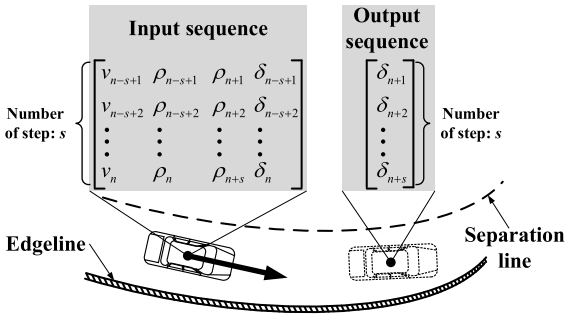

FIGURE 10. Framework of the human-like driver model.

vehicles on free-roads, human drivers' driving behavior mainly depends on their own driving experience and driving habits, and there are no clear desired trajectories in their mind. Normally, the car does not stop abruptly, nor does it move instantaneously. This means the trajectory of the vehicle is continuous, and the steering wheel angle of the driver is also continuous. Since that, the driver model can be built by sequential data modeling approach. At the same time, on free-road, two main factors affecting driver's steering maneuver are vehicle speed and road curvature. So the framework of the human-like driver model is shown as follows:

The inputs of the human-like driver model are historical speeds $[v_{n-s+1}, v_{n-s+2}, \ldots, v_n]$, historical road curvatures $[\rho_{n-s+1}, \rho_{n-s+2}, \ldots, \rho_n]$, future road curvatures $[\rho_{n+1}, \rho_{n+2}, \ldots, \rho_{n+s}]$, and historical steering wheel angles $[\delta_{n-s+1}, \delta_{n-s+2}, \ldots, \delta_n]$. The outputs are future steering wheel angles $[\delta_{n+1}, \delta_{n+2}, \ldots, \delta_{n+s}]$. It is worth noting that s donates the number of step, and it means we want to use standard RNN (or LSTM, GRU) to forecast s steps into the future, based on s steps inputs. The proposed human-like driver model is based on multivariate multi-step standard RNN, LSTM, and GRU.

The first feature of this driver model is that it is modeled directly using the data-driven method based on drivers' steering angles, which maximizes the retention of human driver characteristics, i.e. the model has human-like characteristics. The second feature is that this driver model can utilize both historical information and future information. This is because the steering wheel angles of the drivers on curves can be regarded as sequential data. RNN has unique advantages in modeling sequential data and it has the ability to memorize long-term dependencies. Before modeling, the vehicle speed, steering wheel angle, and road curvature collected from human drivers are transformed into sequential data, see Section VI for details.

1) STANDARD RECURRENT NEURAL NETWORK

As illustrated in Figure 11, the input sequence of the standard RNN network is $x = (x_1, x_2, \ldots, x_n)$, hidden vector sequence $h = (h_1, h_2, \ldots, h_n)$, and output vector sequence $o = (o_1, o_2, \ldots, o_n)$.

The standard RNN hidden layer function is mathematically formulated as follows:

$$h_n = \sigma(W_{hx}x_n + W_{hh}h_{n-1} + b_h). \tag{13}$$

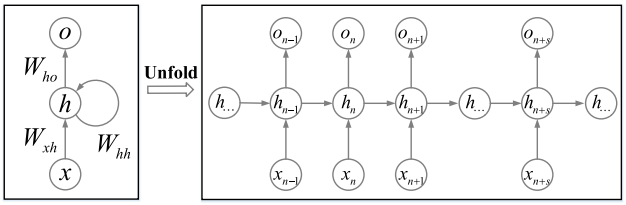

FIGURE 11. Structure of standard RNN.

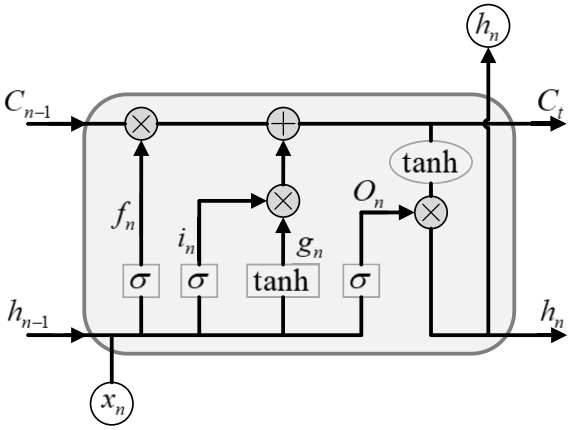

FIGURE 12. Structure of long short term memory neural networks.

And the output is produced by:

$$o_n = W_{oh}h_n + b_o, \tag{14}$$

where $W_*(* = hx, hh, oh)$ represents the weight matrix between each layer, and $b_* = (h, o)$ donates the bias vector. $\sigma(\cdot)$ denotes the standard logistics sigmoid function:

$$\sigma(\cdot) = \frac{1}{1 + e^{-x}}. \tag{15}$$

The standard RNN computes activations for each time-step which makes them extremely deep and may lead to vanishing or exploding gradients.

2) LONG SHORT TERM MEMORY

LSTM is widely applied because it reduces the vanishing and exploding gradient problems and can learn longer term dependencies. The structure of LSTM is shown in Figure 12.

To capture the information from the inputs, the relationship between the input gate i_n, forget gate f_n and output gate o_n as follows:

$$i_n = \sigma(W_{ix}x_n + W_{ih}h_{n-1} + W_{ic}c_{n-1} + b_i), \tag{16}$$
$$f_n = \sigma(W_{fx}x_n + W_{fh}h_{n-1} + W_{fc}c_{n-1} + b_f), \tag{17}$$
$$o_n = \sigma(W_{ox}x_n + W_{oh}h_{n-1} + W_{oc}c_{n-1} + b_o), \tag{18}$$
$$\tilde{c}_n = \tanh(W_{cx}x_n + W_{ch}h_{n-1} + b_c), \tag{19}$$
$$c_n = i_n \odot \tilde{c}_n + f_n \odot c_{n-1}, \tag{20}$$
$$h_n = o_n \odot \tanh(c_n), \tag{21}$$

where $W_*(* = ix, ih, ic, fx, fh, fc, ox, oh, oc, cx, ch)$ donates the weight matrix, $b_*(* = i, f, o, c)$ the bias vector, $\odot$ the scalar product of two vectors, and tanh(·) hyperbolic tangent function:

$$\tanh(x) = \frac{e^x - e^{-x}}{e^x + e^{-x}}. \tag{22}$$

The use of these gates allows LSTM to determine whether to keep existing memory or weigh new information over existing memory, which is a feature that is not present in standard RNN.

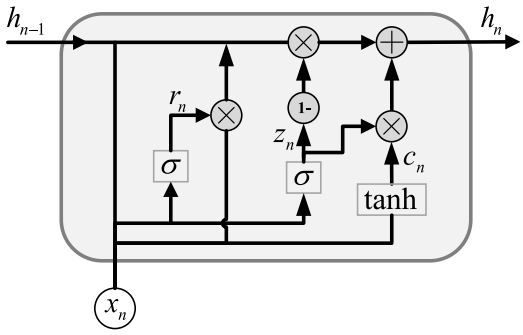

FIGURE 13. Structure of gated recurrent unit neural networks.

3) GATED RECURRENT UNIT

RNN with gated recurrent units (GRU) can be viewed as a light-weight version of LSTM [44].

Similar to the LSTM unit, the GRU also has gating units (reset gate r_n and update gate z_n) that modulate the flow of information inside the unit, however, without having a separate memory cell:

$$r_n = \sigma(W_{rx}x_n + W_{rh}h_{n-1} + b_r), \tag{23}$$
$$z_n = \sigma(W_{zx}x_n + W_{zh}h_{n-1} + b_z), \tag{24}$$
$$\tilde{h}_n = \tanh(W_{\tilde{h}x}x_n + W_{\tilde{h}h}h_{n-1}(r_n \odot h_{n-1}) + b_{\tilde{h}}), \tag{25}$$
$$h_n = (1 - z_n) \odot h_{n-1} + z_n \odot \tilde{h}_n, \tag{26}$$

where $W_*(* = rx, rh, zx, zh, \tilde{h}x, \tilde{h}h)$ donates the weight matrix, and $b_*(* = r, z, \tilde{h})$ the bias vector. The activation of GRU h_n is a linear interpolation between the previous activation h_{n-1} and the candidate activation $\tilde{h}_n$, controlled by the update gate z_n.

C. PERFORMANCE INDEX

The models' prediction performances are evaluated by root mean squared error (RMSE) and mean absolute percentage error (MAPE) [45]:

$$\text{RMSE} = \sqrt{\frac{1}{n}\sum_{i=1}^{n}(\hat{y}_i - y_i)^2}, \tag{27}$$

$$\text{MAPE} = \frac{1}{n}\sum_{i=1}^{n}\left|\frac{\hat{y}_i - y_i}{y_i}\right| \times 100\%. \tag{28}$$

RMSE measures residual error, which gives a global idea of the difference between the observed and modelled values. MAPE has the advantage of being scale-independent, and

TABLE 6. Hyperparameter settings.

Hyperparameter	Value
Input data	$\begin{bmatrix} v_{n-s+1} & \rho_{n-s+1} & \rho_{n+1} & \delta_{n-s+1} \\ v_{n-s+2} & \rho_{n-s+2} & \rho_{n+2} & \delta_{n-s+2} \\ \vdots & \vdots & \vdots & \vdots \\ v_n & \rho_n & \rho_{n+2} & \delta_n \end{bmatrix}$
Output data	$\begin{bmatrix} \delta_{n+1} \\ \delta_{n+2} \\ \vdots \\ \delta_{n+s} \end{bmatrix}$
Historical step s	(5,10,15)
LSTM layers	2
LSTM layer 1 neurons	(50,100)
LSTM layer 2 neurons	(50,100)
Learning rate	0.001
Epoches	1000

therefore are frequently used to compare forecast performance between different scaled datasets.

VIII. RESULT AND DISCUSSION

Three different RNN driver models (standard RNN, LSTM, and GRU) are proposed in this study to establish the human-like driver model of experienced drivers based on field test data.

A. HYPERPARAMETER SETTINGS

The length of experimental road R1, R2, R3, and R4 are 707 m, 318 m, 167 m, and 533 m, separately. Since the lengths of the four roads in the field test are different, this will result in different lengths of the sequence data. In order to make the length of the sequence data obtained from different roads the same, the "pad_sequences()" function in the "Keras" are used to pad variable length sequences.

Standard RNN, LSTM, and GRU models are all composed of 1 input layer, 2 hidden layers, and 1 output layer. We designed two different configuration architectures. First architecture has 50 nodes in each hidden layer whereas the second architecture has 100 nodes in each hidden layer. According to the process method illustrated in Section VII, the obtained vehicle speeds, vehicle positions, road curvature, and steering wheel angles are transformed into sequence data. The inputs of driver models are historical speeds, historical road curvatures, future road curvatures, and historical steering wheel angles, as well as the outputs are future steering wheel angles. Before training, min-max normalization is applied to scale the feature data linearly between 0 and 1. Based on back propagation through time, standard RNN, LSTM, and GRU models are trained by Adam optimizer. Besides, the learning rate is 0.001, and the number of epoch is 1000. All the hyperparameter settings are illustrated in Table 6.

In Table 6, s donates the number of historical step and three values (5, 10, and 15) of s are set for the comparison of prediction performances. It is worth noting that the distance between two neighboring virtual landmark is 1 m, when the value of s is 5 (or 10, 15), it means we want to use standard RNN, LSTM, and GRU to forecast outputs of the last 5 m (or 10 m, 15 m), based on inputs of the first 5 m (or 10 m, 15 m). We have implemented the human-like driver model via deep learning library "Keras" (2.2.2) with "Tensorflow" (1.9.0) as back end and the programming language is Python 3.5.

TABLE 7. Prediction performances of the standard RNN, LSTM, and GRU models in validation period.

			RMSE	MAPE(%)
$h_{50} \times h_{50}$	RNN	$s = 5$	0.1532	5.4038
		$s = 10$	0.1307	3.7477
		$s = 15$	0.1177	4.2788
	LSTM	$s = 5$	0.0846	4.3948
		$s = 10$	0.0723	**1.3641**
		$s = 15$	0.0699	3.1084
	GRU	$s = 5$	0.0872	4.1320
		$s = 10$	0.0821	2.4946
		$s = 15$	0.0711	2.3461
$h_{100} \times h_{100}$	RNN	$s = 5$	0.1254	4.6654
		$s = 10$	0.1107	3.6776
		$s = 15$	0.0924	3.0907
	LSTM	$s = 5$	0.0818	3.7281
		$s = 10$	0.0633	2.5624
		$s = 15$	**0.0599**	*1.5396*
	GRU	$s = 5$	0.0811	2.0959
		$s = 10$	0.0649	2.1602
		$s = 15$	*0.0603*	2.1431

B. RESULT

We use field test data of the first 14 participants for training, 4 participants for validation, and the remaining 2 participants for testing the generalization ability of the human-like driver model.

1) PREDICTION PERFORMANCES IN VALIDATION PERIOD

We design two kinds of hidden layer neurons of each model: the first kind has two hidden layers, the number of nodes are 50, which is denoted as $h_{50} \times h_{50}$; the second kind also has two hidden layers, but the number of nodes are 100, which is denoted as $h_{100} \times h_{100}$. The prediction performances of the standard RNN, LSTM, and GRU models are illustrated in Table 7. The algorithm with the best performance and the one with the second best performance are marked in bold and italics, respectively.

The minimum value of RMSE is 0.0599, and it belongs to LSTM with $h_{100} \times h_{100}$ hidden structure. When the number of nodes is 100, the prediction performances of standard RNN, LSTM and GRU are generally better than those when the number of hidden layers' nodes is 50. For the comparison of standard RNN, LSTM, and GRU, it can be seen that LSTM gives us the most control-ability and thus, better results. However, LSTM has more complexity and operating cost than GRU and standard RNN. GRU is the light-weight version of LSTM, it can balance both forecasting performance and running cost. It is also worth noting that with the increase of s, RMSEs of the three RNN models decrease gradually. For MAPE, the minimum value is 1.3641%, and the maximum value is 5.4038%. Overall, the prediction accuracy of the

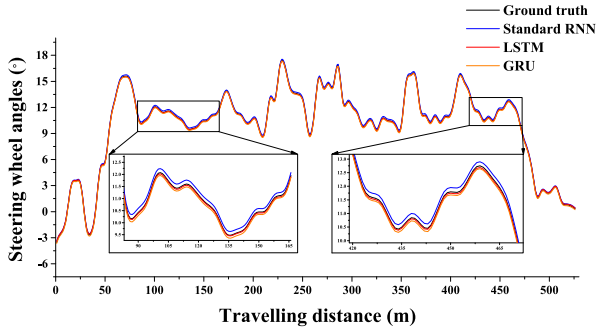

FIGURE 14. Comparison of prediction results of standard RNN, LSTM, and GRU.

three RNN-based human-like driver models is very high. The high prediction accuracy indicates that the RNN-based driver models are very similar to the human driver's driving behavior. Combining with the comparisons of DTW results between preview-based driver models and human drivers, it can be concluded that the steering wheel angles of the human-like driver models proposed in this paper are closer to the actual steering wheel angles of the human drivers on curved roads.

2) PREDICTION PERFORMANCES IN TESTING PERIOD

The last 2 participants' driving data are used for testing the generalization ability of human-like driver model. The experienced drivers' steering wheel angles on the four curved road are regarded as ground truth. Figure 14 illustrates one piece of the prediction results of three RNN-based driver models.

In Figure 14, the specified speed is 50 km/h, the historical step s is 10 and the configuration architectures is $h_{100} \times h_{100}$, and the ground truth is the steering wheel angles of driver J19 on experimental road R4. Generally speaking, the predicted results of the three RNN-based driver models are very close to ground truth. However, from the two local enlarged drawings, the steering wheel angles predicted by LSTM model are the closest to those of human drivers.

In order to further study the humanoid degree of RNN-based models, we also use DTW to compare the similarities of steering wheel angles in Figure 14. The similarity between the ground truth and the standard RNN $DTW_{GT,RNN}$ (GT is donated for ground truth) is 0.0946. The similarities between the ground truth and the LSTM $DTW_{GT,LSTM}$, as well as GRU $DTW_{GT,GRU}$ are 0.0228 and 0.0726, respectively.

Figure 15 shows the prediction performances of the of the standard RNN, LSTM, and GRU driver models, and the configuration architectures of all the three models are $h_{100} \times h_{100}$.

Similar to the prediction performance in validation period, the prediction results of LSTM model are the closest to the ground truth. However, compared with validation period, RMSE and MAPE increase slightly in test period. So far, the RNN-based driver model demonstrates very high prediction accuracy. This means that the RNN-based driver

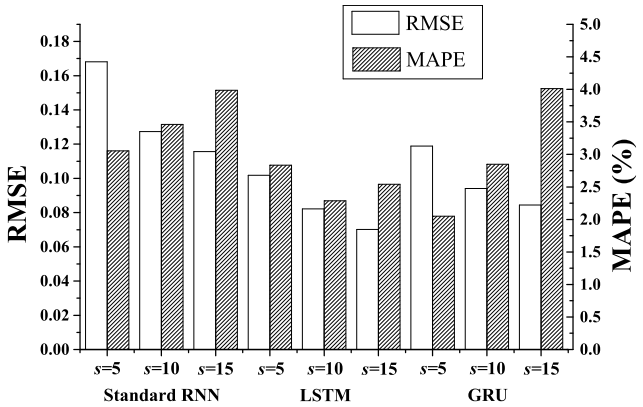

FIGURE 15. Prediction performances of the of the standard RNN, LSTM, and GRU driver models.

models proposed in this paper not only have strong generalization performance, but also achieve the goal of human-like. Another point to note is that, the LSTM model is the best performing model. In short, the LSTM-based human-like driver model can generate steering wheel angles that are very similar to human drivers on curves, enabling human-like driving experience.

IX. CONCLUSION

In this study, three preview-based driver models (including single-point preview, two-point preview, and multi-point preview driver models) were simulated in PreScan+Simulink with a 2-dof vehicle model. To find the most similar pair of steering wheel angles between simulation results and experienced drivers, DTW was introduced. The calculation results showed that there were big differences between preview-based models and experienced drivers, and preview-based driver models were difficult to reflect different driving habits and driving characteristics of different human drivers. For making AVs behave more like human drivers, we proposed a human-like driver with recurrent neural networks. Twenty experienced drivers took part in the field test and the experimental vehicle was equipped with GPS/INS and MSW. The experienced drivers' steering wheel angles, vehicle locations, vehicle speeds, and road curvatures were collected on four two-lane curved roads under four specified speeds.

Then, by setting virtual landmarks along the separation line of each experimental road, all the driving data we collected were transformed into sequential data with a uniform format. Based on multivariate multi-step standard RNN, LSTM, and GRU, the human-like driver model was established directly by experienced drivers' driving data. We designed two hidden layer neurons with one was 50 and the other was 100. We also selected three historical steps ($s = 5, 10, 15$) to compare the prediction performances of different RNN-based models. The inputs of human-like driver models were historical speeds, historical road curvatures, future road curvatures, and historical steering wheel angles, as well as the outputs were future steering wheel angles.

Through comparing the prediction results with RMSE, MAPE, and DTW, it shows that LSTM driver model has the best prediction performance in validation period. What's more, the last 2 participants' driving data are used for testing the generalization ability of the human-like driver model. The calculation results of performance index show that, the human-like driver model established in this paper can generate human-like steering wheel angles on curved roads.

Driver model is a expression of driving behavior, but we know that human driving behavior is complicated, uncertain, and has personalized differences. From the analysis and comparison results in this paper, it can be seen that preview-based driver models are difficult to describe different human drivers with different driving styles. Compared with physical model, the driver model built using data-driven methods (e.g. RNN-based approaches in this study) may be more suitable for human-like implementation.

The human-like driver model on free curved roads is a basic model, and it needs to work with other algorithms in more complex traffic scenarios. On the one hand, the human-like driver model in this paper mainly involves the generation of human-like steering wheel angles, and does not control the vehicle speed. For example, when AVs are in car-following scenario, the human-like driver model needs to be used with speed control model. On the other hand, if AVs want to change lanes, the human-like driver model needs to be improved with the combination of other lane-changing algorithms. In this way, the human-like driver model will make AVs drive on curves really like human drivers.

REFERENCES

[1] L. Xu and G. Mcardle, "Internet of too many things in smart transport: The problem, the side effects and the solution," *IEEE Access*, vol. 6, pp. 62840–62848, 2018.

[2] W. Qu, J. Xu, Y. Ge, X. Sun, and K. Zhang, "Development and validation of a questionnaire to assess public receptivity toward autonomous vehicles and its relation with the traffic safety climate in china," *Accident Anal. Prevention*, vol. 128, pp. 78–86, Jul. 2019.

[3] L. M. Hulse, H. Xie, and E. R. Galea, "Perceptions of autonomous vehicles: Relationships with road users, risk, gender and age," *Saf. Sci.*, vol. 102, pp. 1–13, Feb. 2018.

[4] A. Li, H. Jiang, J. Zhou, and X. Zhou, "Learning human-like trajectory planning on urban two-lane curved roads from experienced drivers," *IEEE Access*, vol. 7, pp. 65828–65838, 2019.

[5] M. Scheutz, "The need for moral competency in autonomous agent architectures," in *Fundamental Issues of Artificial Intelligence*, V. C. Müller, Ed. Cham, Switzerland: Springer, 2016, pp. 517–527.

[6] C. You, J. Lu, and P. Tsiotras, "Nonlinear driver parameter estimation and driver steering behavior analysis for ADAS using field test data," *IEEE Trans. Human-Mach. Syst.*, vol. 47, no. 5, pp. 686–699, Oct. 2017.

[7] C. Macadam, "An optimal preview control for linear systems," *ASME J. Dyn. Syst., Meas. Control*, vol. 102, pp. 188–190, Sep. 1980.

[8] M. Plöchl and E. Johannes, "Driver models in automobile dynamics application," *Veh. Syst. Dyn.*, vol. 45, no. 7, pp. 699–741, 2007.

[9] D. J. Cole, A. J. Pick, and A. M. C. Odhams, "Predictive and linear quadratic methods for potential application to modelling driver steering control," *Vehicle Syst. Dyn.*, vol. 44, no. 3, pp. 259–284, 2006.

[10] S. Schnelle, J. Wang, H.-J. Su, and R. Jagacinski, "A personalizable driver steering model capable of predicting driver behaviors in vehicle collision avoidance maneuvers," *IEEE Trans. Human-Mach. Syst.*, vol. 47, no. 5, pp. 625–635, Oct. 2017.

[11] C. C. MacAdam and G. E. Johnson, "Application of elementary neural networks and preview sensors for representing Driver steering control behaviour," *Veh. Syst. Dyn.*, vol. 25, no. 1, pp. 3–30, 1996.

[12] A. El Hajjaji and M. Ouladsine, "Modeling human vehicle driving by fuzzy logic for standardized iso double lane change maneuver," in *Proc. IEEE 10th Int. Workshop Robot Hum. Interact. Commun. (ROMAN)*, Sep. 2001, pp. 499–503.

[13] J. Krumm, "A Markov model for driver turn prediction," in *Proc. Soc. Automot. Eng. SAE World Congr.*, Apr. 2008.

[14] Y. Park, J. H. Yang, and S. Lim, "Development of complexity index and predictions of accident risks for mixed autonomous driving levels," in *Proc. IEEE Int. Conf. Syst., Man, Cybern. (SMC)*, Oct. 2018, pp. 1181–1188.

[15] F. Petitjean, A. Ketterlin, and P. Gançarski, "A global averaging method for dynamic time warping, with applications to clustering," *Pattern Recognit.*, vol. 44, no. 3, pp. 678–693, Mar. 2011.

[16] C. J. Nash, D. J. Cole, and R. S. Bigler, "A review of human sensory dynamics for application to models of driver steering and speed control," *Biological*, vol. 110, pp. 91–116, Jun. 2016.

[17] J. Cao, H. Lu, K. Guo, and J. Zhang, "A driver modeling based on the preview-follower theory and the jerky dynamics," *Math. Problems Eng.*, vol. 2013, Nov. 2013, Art. no. 952106.

[18] D. D. Salvucci and R. Gray, "A two-point visual control model of steering," *Perception*, vol. 33, no. 10, pp. 1233–1248, 2004.

[19] R. S. Sharp, D. Casanova, and P. Symonds, "A mathematical model for driver steering control, with design, tuning and performance results," *Veh. Syst. Dyn.*, vol. 33, no. 5, pp. 289–326, 2000.

[20] L.-K. Chen and A. G. Ulsoy, "Identification of a driver steering model, and model uncertainty, from driving simulator data," *J. Dyn. Syst., Meas., Control*, vol. 123, no. 4, pp. 623–629, 2001.

[21] J. Steen, H. J. Damveld, R. Happee, M. M. van Paassen, and M. Mulder, "A review of visual driver models for system identification purposes," in *Proc. IEEE Int. Conf. Syst., Man, Cybern.*, Oct. 2011, pp. 2093–2100.

[22] Y. W. Chai, Y. Abe, Y. Kano, and M. Abe, "A study on adaptation of SBW parameters to individual driver's steer characteristics for improved driver–vehicle system performance," *Vehicle Syst. Dyn.*, vol. 44, pp. 874–882, Apr. 2006.

[23] J. Ishio, H. Ichikawa, Y. Kano, and M. Abe, "Vehicle-handling quality evaluation through model-based driver steering behaviour," *Vehicle Syst. Dyn.*, vol. 46, no. S1, pp. 549–560, 2008.

[24] L. Chong, M. M. Abbas, A. M. Flintsch, and B. Higgs, "A rule-based neural network approach to model driver naturalistic behavior in traffic," *Transp. Res. C, Emerg. Technol.*, vol. 32, pp. 207–223, Jul. 2013.

[25] D. F. Llorca, V. Milanes, I. P. Alonso, M. Gavilan, I. G. Daza, J. Perez, and M. Á. Sotelo, "Autonomous pedestrian collision avoidance using a fuzzy steering controller," *IEEE Trans. Intell. Transp. Syst.*, vol. 12, no. 2, pp. 390–401, Jun. 2011.

[26] Y. Lin, P. Tang, W. J. Zhang, and Q. Yu, "Artificial neural network modelling of driver handling behaviour in a driver-vehicle-environment system," *Int. J. Vehicle Des.*, vol. 37, no. 1, pp. 24–45, 2005.

[27] Y. Cao, J. Cao, F. Yu, and Z. Luo, "A new vehicle path-following strategy of the steering driver model using general predictive control method," *Proc. Inst. Mech. Eng., C, J. Mech. Eng. Sci.*, vol. 232, no. 24, pp. 4578–4587, 2018.

[28] S. M. Erlien, S. Fujita, and J. C. Gerdes, "Shared steering control using safe envelopes for obstacle avoidance and vehicle stability," *IEEE Trans. Intell. Transp. Syst.*, vol. 17, no. 2, pp. 441–451, Feb. 2016.

[29] A. Y. Ungoren and H. Peng, "An adaptive lateral preview driver model," *Vehicle Syst. Dyn.*, vol. 43, no. 4, pp. 245–259, 2005.

[30] S. D. Keen and D. J. Cole, "Application of time-variant predictive control to modelling driver steering skill," *Vehicle Syst. Dyn.*, vol. 49, no. 4, pp. 527–559, 2011.

[31] M. Bojarski, D. D. Testa, D. Dworakowski, B. Firner, B. Flepp, P. Goyal, L. D. Jackel, M. Monfort, U. Müller, J. Zhang, X. Zhang, J. Zhao, and K. Zieba, "End to end learning for self-driving cars," Apr. 2016, *arXiv:1604.07316*. [Online]. Available: https://arxiv.org/abs/1604.07316

[32] L. Chi and Y. Mu, "Deep steering: Learning end-to-end driving model from spatial and temporal visual cues," Aug. 2017, *arXiv:1708.03798*. [Online]. Available: https://arxiv.org/abs/1708.03798

[33] L. Cardamone, D. Loiacono, and P. L. Lanzi, "Learning drivers for TORCS through imitation using supervised methods," in *Proc. IEEE Symp. Comput. Intell. Games*, Sep. 2009, pp. 148–155.

[34] Y. Jia, J. Wu, M. Ben-Akiva, R. Seshadri, and Y. Du, "Rainfall-integrated traffic speed prediction using deep learning method," *IET Intell. Transport Syst.*, vol. 11, no. 9, pp. 531–536, Nov. 2017.

[35] C. Yin, Y. Zhu, J. Fei, and X. He, "A deep learning approach for intrusion detection using recurrent neural networks," *IEEE Access*, vol. 5, pp. 21954–21961, 2017.

[36] X. Huang, J. Sun, and J. Sun, "A car-following model considering asymmetric driving behavior based on long short-term memory neural networks," *Transp. Res. C, Emerg. Technol.*, vol. 95, pp. 346–362, Oct. 2018.
[37] J. Zhao, Y. Gao, Y. Qu, H. Yin, Y. Liu, and H. Sun, "Travel time prediction: Based on gated recurrent unit method and data fusion," *IEEE Access*, vol. 6, pp. 70463–70472, 2018.
[38] H. Jiang, K. Shi, J. Cai, and L. Chen, "Trajectory planning and optimisation method for intelligent vehicle lane changing emergently," *IET Intell. Transp. Syst.*, vol. 12, no. 10, pp. 1336–1344, 2018.
[39] A. M. C. Odhams and D. J. Cole, "Application of linear preview control to modelling human steering control," *Proc. Inst. Mech. Eng., D, J. Automobile Eng.*, vol. 223, no. 7, pp. 835–853, 2009.
[40] G. Markkula, O. Benderius, and M. Wahde, "Comparing and validating models of driver steering behaviour in collision avoidance and vehicle stabilisation," *Vehicle Syst. Dyn.*, vol. 52, no. 12, pp. 1658–1680, 2014.
[41] D. Sart, A. Mueen, W. Najjar, E. Keogh, and V. Niennattrakul, "Accelerating dynamic time warping subsequence search with GPUs and FPGAs," in *Proc. IEEE Int. Conf. Data Mining*, Dec. 2010, pp. 1001–1006.
[42] O. Lappi, E. Lehtonen, J. Pekkanen, and T. Itkonen, "Beyond the tangent point: Gaze targets in naturalistic driving," *J. Vis.*, vol. 13, pp. 1–18, Nov. 2013.
[43] O. Lappi, "Future path and tangent point models in the visual control of locomotion in curve driving," *J. Vis.*, vol. 14, no. 12, pp. 1–22, Oct. 2014.
[44] X.-Y. Zhang, F. Yin, Y.-M. Zhang, C.-L. Liu, and Y. Bengio, "Drawing and recognizing Chinese characters with recurrent neural network," *IEEE Trans. Pattern Anal. Mach. Intell.*, vol. 40, no. 4, pp. 849–862, Apr. 2018.
[45] M. V. Shcherbakov, A. Brebels, N. L. Shcherbakova, A. P. Tyukov, T. A. Janovsky, and V. A. Kamaev, "A survey of forecast error measures," *World Appl. Sci. J.*, vol. 24, no. 24, pp. 171–176, 2013.

AOXUE LI received the B.S. and M.S. degrees in vehicle engineering from Jiangsu University, Zhenjiang, China, in 2013 and 2016, respectively, where he is currently pursuing the Ph.D. degree in vehicle engineering. Since August 2018, he has been a Visiting Scholar with the Department of Mechanical Engineering, Michigan State University, East Lansing, MI, USA. His research interests include the autonomous vehicle, intelligent transportation system, and ADAS technologies.

HAOBIN JIANG received the B.S. degree in agricultural mechanization from Nanjing Agricultural University, Nanjing, China, in 1991, and the M.S. and Ph.D. degrees in vehicle engineering from Jiangsu University, Zhenjiang, China, in 1994 and 2000, respectively.

From 1994 to 1995, he was a Research Assistant with the Laboratory of Power and Energy, Faculty of Biological Resources, Mie University, Mie, Japan. He joined Jiangsu University, Zhenjiang, China, in 1994, where he is currently a Professor of vehicle engineering. He is the Steering Technology Committee Member of the Society of Automotive Engineering of China, the Steering Technology Committee Member of the National Technical Committee of Auto Standardization, China, and the Standing Director of the Society of Automotive Engineering of Jiangsu. He is also the Dean of the School of Automotive and Traffic Engineering, Jiangsu University. His research interests include vehicle dynamic performance analysis and electrical control technology, active safety control techniques and theories of road vehicles, and intelligent transportation technology.

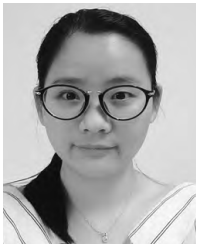

JIE ZHOU received the B.S. degree in vehicle engineering from Jiangsu University, Zhenjiang, China, in 2016, where she is currently pursuing the M.S. degree with the Department of Traffic and Transportation Engineering. Her research interests include the autonomous vehicle and intelligent transportation systems.

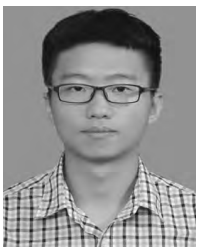

XINCHEN ZHOU received the B.S. degree in vehicle engineering from Jiangsu University, Zhenjiang, China, in 2017, where he is currently pursuing the M.S. degree with the Department of Vehicle Engineering. His research interests include automatic parking and intelligent automobile.